Anal Bioanal Chem (2005) 381: 1299–1304
DOI 10.1007/s00216-005-3068-9

TECHNICAL NOTE

**Myeong Hee Moon · Sung Gwon Yang
Jae Young Lee · Seungho Lee**

# Combination of gravitational SPLITT fractionation and field-flow fractionation for size-sorting and characterization of sea sediment

Received: 2 October 2004 / Revised: 16 December 2004 / Accepted: 20 December 2004 / Published online: 3 March 2005


**Abstract** A combination of gravitational split-flow thin (SPLITT) fractionation and sedimentation/steric field-flow fractionation (Sd/StFFF) has been used for continuous size-sorting of a sediment sample and for size analysis of the collected fractions. An IAEA (International Atomic Energy Agency) sediment material was separated into four size fractions (with theoretical size ranges $<1.0$, 1.0–3.0, 3.0–5.0, and $>5.0$ μm in diameter) by means of a three-step gravitational SPLITT fractionation (GSF) for which the same GSF channel was used throughout. The GSF fractions were collected and examined by optical microscopy (OM) and by Sd/St FFF. The mean diameters of the GSF fractions measured by OM were within the size interval predicted by GSF theory, despite the theory assuming that all particles are spherical, which is not true for the sediment particles. The Sd/St FFF results showed that retention shifted toward shorter elution time (or larger size) than expected, probably because of the shape effect. The results from GSF, OM, and Sd/StFFF are discussed in detail.

**Keywords** SPLITT · Gravitational SPLITT fractionation · Field-flow fractionation · Sedimentation/steric FFF · Sea sediment · Size characterization · Particle sorting

M. H. Moon
Department of Chemistry,
Yonsei University, Seoul, 120-749,
South Korea
E-mail: mhmoon@yonsei.ac.kr
Tel.: +82-2-21235634

S. G. Yang · J. Y. Lee · S. Lee (✉)
Department of Chemistry,
Hannam University,
Taejon, 306-791, South Korea
E-mail: slee@hannam.ac.kr
Tel.: +82-42-6297473

## Introduction

Gravitational split-flow thin fractionation (or gravitational SPLITT fractionation, GSF) is a rapid and preparative-scale separation technique capable of fractionating particles or macromolecules into two or more fractions by utilizing gravitational force applied perpendicular to the flow direction [1–6]. Similar to field-flow fractionation (FFF) techniques, separation in GSF is generally performed in a thin rectangular channel as shown in Fig. 1.

In a typical GSF channel, two inlet sub-streams are introduced into the channel through two inlets (the sample inlet a′ and the carrier inlet b′) which are separated by the inlet splitter as shown in Fig. 1. Particles are continuously fed into the channel through the sample inlet a′. Usually the volumetric flow rate of the carrier inlet, $\dot{V}(b')$ is much higher than that of the sample inlet, $\dot{V}(a')$and thus compresses the sample feed lamina toward the upper channel wall, as shown by the inlet-splitting plane (ISP) in Fig. 1. A thin layer of the sample is thus formed close to the upper wall of the channel; its thickness is equal to the distance between ISP and the upper channel wall. The lateral position of ISP, and thus the thickness of the sample layer, depends on the flow rate ratio, $\dot{V}(a')/\dot{V}(b')$ [1, 2]. As the ratio decreases, the thickness of the sample layer decreases.

After the formation of the thin layer the particles are carried down the channel toward the channel exit by the merged flow; at the same time they settle under the action of gravitational force. At the end of the GSF channel, particles having different sedimentation coefficients are distributed along the direction of the gravitational force [1]. Particles of a larger effective mass (or size, in the case of uniform density) have a higher sedimentation coefficient and settle faster than those of a smaller mass. Near the channel exits, the outlet-splitting plane (OSP) is formed; its lateral position depends on the ratio of the upper to lower exit flow rates, $\dot{V}(a)/\dot{V}(b)$. Particles having sedimentation coefficients

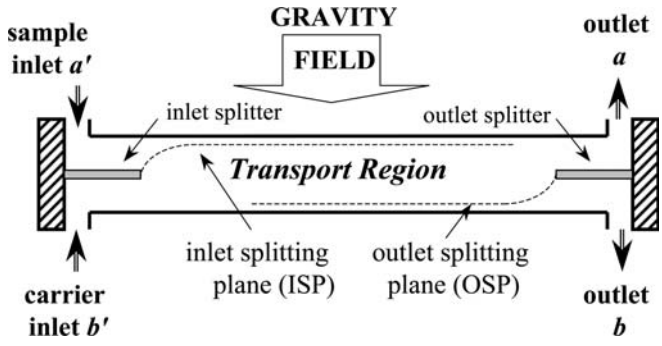


**Fig. 1** Schematic side view of GSF channel

high enough to cross the OSP exit through the lower outlet (outlet b) whereas the others exit through the upper outlet (outlet a). GSF thus enables fractionation of the sample particles into two fractions based on the sedimentation coefficient, and thus on the mass or the size.

One of the merits of GSF is that the particles can be fed into the channel continuously, enabling fractionation on a preparative scale. For spherical particles the cut-off diameter, $d_c$, is given by [1, 7, 8]:

$$d_{\mathrm{c}} = \sqrt{\frac{18\eta(\dot{V}(\mathrm{a}) - 0.5\dot{V}(\mathrm{a}'))}{bLG(\rho_{\mathrm{p}} - \rho)}} \qquad (1)$$

where $\dot{V}(a')$ and $\dot{V}(a)$are the volumetric flow rate entering through the sample inlet a′, and exiting through the upper outlet b′, respectively, $\eta$ the viscosity of carrier liquid, $b$ the channel breadth, $L$ the channel length, $G$ gravity, and $\Delta\rho$ the density difference between the sample and carrier liquid. According to Eq. 1, $d_c$ can be adjusted by controlling $\dot{V}(a')$ and $\dot{V}(a)$. GSF can be used to remove oversized particles at a desired cut-off diameter or to separate particles into several fractions by fractionating the previously collected GSF fractions again under different flow rate conditions.

In this study, GSF was combined with sedimentation/steric field-flow fractionation (Sd/StFFF) for fractionation then characterization of a sediment material. GSF was used for fractionation of the sediment into four size groups and Sd/StFFF for analysis of the particle-size distribution of the fractions.

SdFFF, one of the subtechniques of FFF, is an elution-based analytical method capable of separating various particulate materials (e.g. nano-particles, colloids, inorganic particles, cells, etc.) in the size range from nanometers to approximately 100 μm [9–13]. SdFFF is carried out in a thin ribbon-like rectangular channel with centrifugal acceleration force applied in the direction perpendicular to the channel flow. As described in earlier publications [14–18], separation in SdFFF is achieved by differential distribution of sample components of different size against the bottom wall of the channel. The distribution of particles is established as a result of the equilibrium between the two counteracting forces exerted on the components:

1. the sedimentation force driving the sample components toward the bottom wall of the channel, and
2. the Brownian motion in the normal mode or the hydrodynamic lift forces in the steric mode pushing the components away from the wall.

Sd/StFFF is useful for separation and size-analysis of particles larger than approximately 1 μm [19]. It enables rapid, high resolution separation of particles, with elution in order of decreasing particle size [20, 21].

In earlier work a modified GSF channel was used to fractionate marine sediments on a semi-preparative scale; GSF channels of different dimensions were used for fractionations at different cut-off diameters [22]. In this study a single GSF channel was used throughout the entire GSF fractionation procedure. Also, both the sample and carrier-inlet flow rates were fixed constant, so that the position of the ISP was fixed. The cut-off diameters were controlled by adjusting the upper ($\dot{V}(a)$) and lower ($\dot{V}(b)$) outlet-flow rates as given by Eq. 1. GSF was used to fractionate IAEA sediment particles into four subpopulations with theoretical size ranges $<1.0$, 1.0–3.0, 3.0–5.0, and $>5.0$ μm in diameter. The size distributions of the GSF fractions were analyzed by optical microscopy (OM) and by Sd/StFFF.

## Experimental

### Gravitational SPLITT fractionation

A GSF channel system was constructed in-house with a 127-μm-thick stainless steel splitter sandwiched between two Mylar spacers of the same thickness (resulting in the channel thickness of 381 μm). The channel breadth ($b$) was 4.0 cm and the length ($L$) 20 cm.

### Sea sediment material

A sea sediment material, IAEA-SED-1, was obtained from the International Atomic Energy Agency (IAEA). The sediment standard (density 2.10 g cm$^{-3}$) was suspended at 0.5 and 1% ($w/v$) in distilled, deionized water containing 0.1% ($w/v$) FL-70 (Fisher Scientific, Fair Lawn, NJ, USA) for particle dispersion and 0.02% sodium azide for bactericide. Two different sample concentrations were tested for comparison. The suspended sample was fed into the channel through inlet a′ by means of a Minipulse-3 peristaltic pump (Gilson Medical Electronics, Middletown, WI, USA). Carrier liquid was the same as the suspension liquid, and was pumped into the channel through inlet b′ by using a model M930 HPLC pump (Young-Lin, Seoul, Korea). The GSF fractions were examined by OM

(Jena Laboval 4, Germany) at a magnification of 400×.

### Sedimentation/steric field-flow fractionation

GSF fractions were analyzed by Sd/StFFF. The SdFFF system was similar to that used in earlier publications [21, 22]. The SdFFF channel was made with a Mylar spacer, which was cut into a ribbon-like shape, clamped between two Hastelloy C stainless-steel plates. The channel was of length ($L$) 90 cm, breadth ($b$) 1.5 cm, and thickness ($w$) 190 μm, which was equal to the thickness of the Mylar spacer from which the channel was cut. The radius ($r$) of the channel rotor was 15.1 cm. The SdFFF carrier liquid was the same as that used in GSF and was delivered into the SdFFF channel by means of a Young-Lin Model 930 HPLC pump. Particles eluted from the SdFFF channel were monitored by means of a Shimadzu SPD-6A UV detector (Tokyo, Japan) at a wavelength of 254 nm. Polystyrene latex spheres of nominal diameter 45.6, 21.4, 9.8, 4.5, and 1.53 μm (density 1.05 g cm$^{-3}$), from Duke Scientific (Palo Alto, CA, USA), were used for calibration.

## Results and discussion

### GSF fractionation of sediment material

Continuous GSF was used to fractionate the IAEA sediment material into four size fractions. As mentioned earlier, the resolution increases as the ratio, $\dot{V}(a')/\dot{V}(b')$ decreases [1, 2]. In this work, $\dot{V}(a')$ and $\dot{V}(b')$ were fixed constant at 1.0 and 9.0 mL min$^{-1}$, respectively, for all GSF operations. By adopting the ratio $\dot{V}(a')/\dot{V}(b')$ 1:9 the particles are expected to form an effectively compressed initial band whose thickness is 10% of the channel thickness, which is 38.1 μm. At a ratio lower than 1:9 it was difficult to feed the sample suspension into the channel because of high back-pressure caused by relatively high $\dot{V}(b')$.

First, GSF was performed to cut the sample at a cut-off diameter of 3.0 μm. With $d_c = 3.0$ μm and $\dot{V}(a') = 1$ mL min$^{-1}$, Eq. 1 gives $\dot{V}(a) = 3.1$ mL min$^{-1}$. The feed concentration of the sample suspension was 0.5% ($w/v$). This first step yields two fractions: "fraction a" collected at outlet a, and "fraction b" collected at outlet b. Both fractions a and b were concentrated by centrifugation for further GSF fractionation. The second step of GSF was then performed to fractionate fraction a at a cut-off diameter of 1.0 μm, which again yields two fractions: "fraction aa" collected at outlet a and "fraction ab" collected at outlet b. Finally the third step of GSF was performed to cut fraction b at the cut-off diameter 5.0 μm, which yields "fraction ba" collected at outlet a and "fraction bb" collected at outlet b. This three-step GSF operation yielded four GSF fractions of the sediment sample, fractions aa, ab, ba, and bb. The flow rate conditions used in all three steps of GSF operations are summarized in Table 1.

**Table 1** Experimental conditions for each step of GSF operations for fractionation of sediment and their corresponding cut-off diameter, $d_c$. The same channel (breadth×length = 4×20 cm, thickness = 381 μm) was used for all GSF

| Step | $d_c$ (μm) | $\dot{V}(a')$ (mL min$^{-1}$) | $\dot{V}(b')$ (mL min$^{-1}$) | $\dot{V}(a)$ (mL min$^{-1}$) | $\dot{V}(b)$ (mL min$^{-1}$) |
|---|---|---|---|---|---|
| 1 | 3 | 1.0 | 9.0 | 3.1 | 6.9 |
| 2 | 1 | 1.0 | 9.0 | 0.8 | 9.2 |
| 3 | 5 | 1.0 | 9.0 | 7.7 | 2.3 |

In theory, fractions aa, ab, ba, and bb are expected to contain particles in the diameter ranges $<1.0$, 1.0–3.0, 3.0–5.0 and $>5.0$ μm, respectively. All four fractions were examined by OM; micrographs of each fraction and the original sample are shown in Fig. 2. It is apparent from Fig. 2 that the sediment particles are not spherical. Despite this, the apparent size gradually increases from fraction aa to bb (four micrographs at the bottom of Fig. 2) as expected from theory.

Figure 3 shows the particle-size distributions (PSD) of the original sample (Fig. 3a) and its four GSF fractions (Fig. 3b) determined by OM. Because most of the particles are not spherical, two-dimensional measurement was used, in which the size of each particle was determined by averaging the sizes measured along the $x$ and $y$ coordinates. For the original sample approximately 140 particles were analyzed; 40–50 particles were analyzed for each GSF fraction.

Figure 3a shows the size distribution of the original sample is broad, ranging up to approximately 10 μm. Although some particles larger than 10 μm were found in the original sample (Fig. 2), the number% of those large particles is, apparently, very low, and negligible compared with that of those smaller than 10 μm. The mean diameter of the original sample is 2.3 μm (std. dev. = 1.7 μm) with more than 92% of particles being smaller than 5 μm.

Figure 3b shows the size distributions of fractions aa, ab, ba, and bb in the approximate ranges 0.3–2.0, 0.6–3.3, 1.2–5.4 and 4.8–9.3 μm with mean sizes 0.4 (std. dev. = 0.3), 1.4 (std. dev. = 0.5), 2.5 (std. dev. = 0.9), and 6.4 (std. dev. = 1.5) μm, respectively. Overall, the measured size-ranges of the fractions are in reasonable agreement with theoretical diameter ranges, except for fraction ba. The mean sizes of the fractions are also within the theoretical diameter range, except for fraction ba. Figure 3b shows that fraction ba contains a substantial number of undersized particles ($d_c$ smaller than 3.0 μm), causing the size range of fraction ba to be extended further down to approximately 1.2 μm, and the mean size (2.5 μm) to be pushed out of the theoretical diameter range of 3–5 μm.

There are many possible reasons for the size ranges of the GSF fractions not exactly matching theoretical diameter ranges. These include:

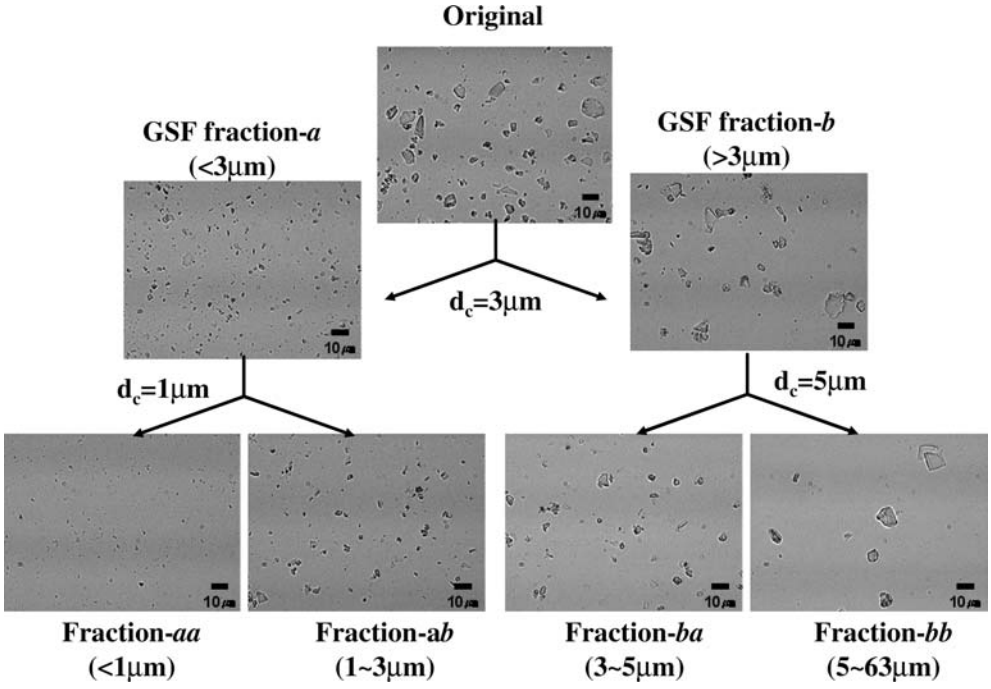


**Fig. 2** GSF scheme for fractionation of IAEA-SED-1 at various cut-off diameters, and optical micrographs of the collected fractions Flow rate conditions are listed in Table 1

1. the sediment particles are not spherical (theoretical diameter range was calculated by assuming the particles are spherical. Non-spherical particles will have sedimentation coefficients different from those of spherical particles of the same apparent diameter, and this will change the observed cut-off diameter from the theoretical value);
2. all the particles were assumed to have a uniform density of 2.1 g $mL^{-1}$, which may not be true;
3. the thin layer of the sample formed at the beginning of GSF channel has a finite thickness, causing particles of the same size to start settling at different lateral positions, which results in co-elution of particles of the same diameter at both outlets;
4. the size distribution determined by OM may not be accurate because only a limited number of particles were measured, 40–50 particles for each fraction;
5. splitter imperfection (e.g. misalignment, surface roughness, and edge discontinuity) could cause flow perturbation; and
6. diffusion of small particles, etc.

All these possible causes of deviation should affect all three GSF steps equally. For example, the thickness of the initial sample layer is identical in all three GSF steps because $\dot{V}(a')$ and $\dot{V}(b')$ were fixed constant at 1 and 9 mL $min^{-1}$, respectively, in all three GSF steps (Table 1).

The high end of the size range of fraction ba is 5.4 μm and the low end of fraction bb is 4.8 μm. Both are close to the theoretical $d_c$ of 5 μm, indicating that GSF step 3 (fractionation of fraction b) performed reasonably well. In fact, fraction bb contains only about 7% (in number) of particles smaller than 5.0 μm.

It seems that the larger deviation of fraction ba was caused by contamination of fraction b by particles smaller than the theoretical $d_c$ of 3 μm at GSF step 1. Although $\dot{V}(a')$ and $\dot{V}(b')$ were fixed constant for all GSF steps, $\dot{V}(a)$ and $\dot{V}(a)$ were different for different GSF steps. For step 1, $\dot{V}(a) = 3.1$, $\dot{V}(a) = 6.9$, whereas for step 3, $\dot{V}(a) = 7.7$, $\dot{V}(b) = 2.3$ mL $min^{-1}$. Thus the height of the OSP from the channel bottom is three-times higher at step 1 than at step 3. If any particles leave their ''ideal'' trajectories, for one or more reasons mentioned above, the possibility of contamination of fraction b by undersized particles (smaller than the cut-off diameter) would be higher for higher OSP.

The ''number % recovery'' was determined for each GSF fraction by counting the number of particles whose sizes were in the theoretical diameter range, and was 66.3, 85.5, 36.1, and 93.1% for fractions aa, ab, ba, and bb, respectively. Although recovery of fractions collected from outlet a (fractions aa and ba) was relatively low, recovery was good (>85%) for fractions collected from outlet b. This is in agreement with GSF results reported previously [5, 7, 8, 23].

Similar results were obtained when the feed concentration was increased to 1%, as shown in Fig. 3c. The mean diameters of fractions aa, ab, ba, and bb were 0.6 (std. dev. = 0.2), 1.6 (std. dev. = 0.5), 2.6 (std. dev. = 0.9), and 7.0 (std. dev. = 1.8), respectively. These values are quite close to those obtained with a feed concentration of 0.5% with the exception of fraction aa.

The four GSF fractions were analyzed by Sd/StFFF, in which the particle equilibrium position in Sd/StFFF is determined by the balance between the driving force (centrifugal acceleration force) and the opposing hydrodynamic lift forces. The hydrodynamic lift forces have

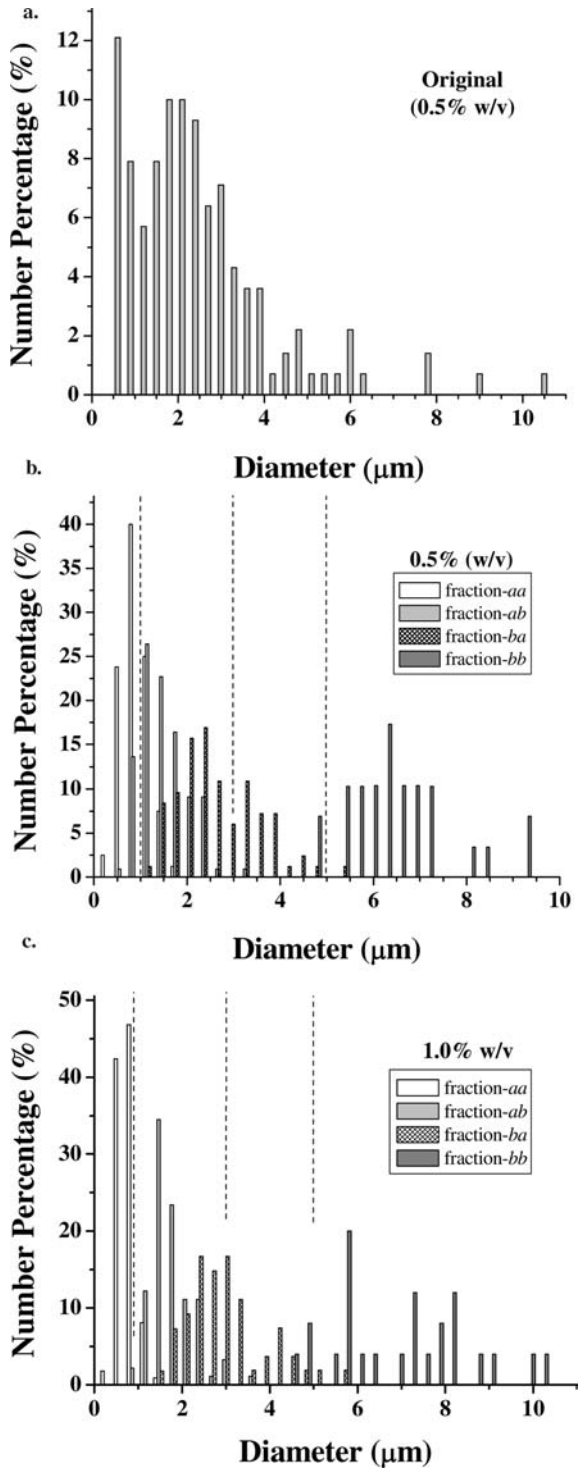


**Fig. 3** Particle-size distributions obtained by microscopic examination of (**a**) the original IAEA-SED-1, (**b**) GSF fractions collected at a feed concentration of 0.5% (*w*/*v*), (**c**) GSF fractions collected at a feed concentration of 1.0% (*w*/*v*). The *dotted lines* represent the position of each cut-off diameter

not yet been clearly understood, and thus the particle size analysis is generally carried out using an empirical calibration procedure [20, 21]. Calibration is based on the linear relationship between the logarithm of the retention time, log $t_r$, and logarithm of the particle diameter, log $d$. Figure 4 shows the Sd/StFFF fractogram (UV detector signal at 254 nm) showing separation of polystyrene latex beads of the indicated diameters obtained with a flow rate of 7.0 mL $min^{-1}$ and at 1,430 rpm (345.6×$g$). It demonstrates the capability of Sd/StFFF for separation of particles ranging from 46 to 1.5 μm. The inset in Fig. 4 shows the corresponding calibration curve, representing a good linear relationship, as expected. The linear calibration is described by the relationship; log $t_r = -S_d$ log $d$ + log $t_{r1}$ where the calibration constants $S_d$ and $t_{r1}$ are the slope of the curve representing the diameter-based selectivity and the extrapolated retention time of a unit-diameter particle, respectively. Experimental values of $S_d$ and $t_{r1}$ for the calibration curve shown in Fig. 4 were 0.69 and 29.9 min, respectively. By utilizing this relationship, particle diameter and its distribution can be determined from retention times in the experimental fractogram.

Because of the different densities of the polystyrene standard particles and the sample particles (sediments in this study), the field strength to be used for sample analysis should be adjusted by the "density-compensation method" [20, 21] so that the effective field strengths exerted on both the calibration standard and the sample are identical: $(G\Delta\rho)_{standard} = G\Delta\rho)_{sample}$ where $G$ is the centrifugal acceleration force ( $\propto$ $rpm^2$) and $\Delta\rho$ is the density difference between the carrier liquid and sample. For density-compensation the original sediment sample and the four fractions obtained from it were analyzed at 300 rpm (equivalent to 1,430 rpm for polystyrene standard). The Sd/StFFF fractograms are shown in Fig. 5 marked with the diameter scale based on the calibration.

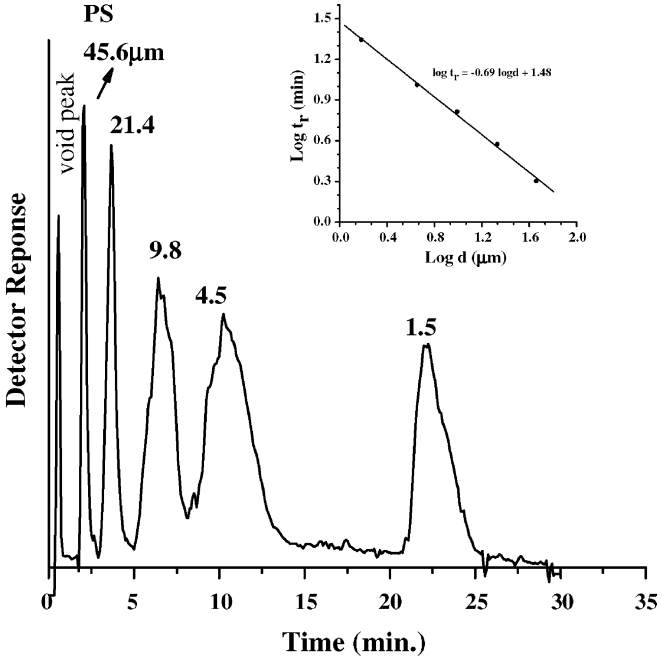


**Fig. 4** Sd/StFFF separation of a mixture of five polystyrene latex spheres obtained at a rotation speed of 1,430 rpm and a flow rate of 7.0 mL $min^{-1}$. The *inset* is the calibration curve representing the linear relationship between log $t_r$ and log $d$

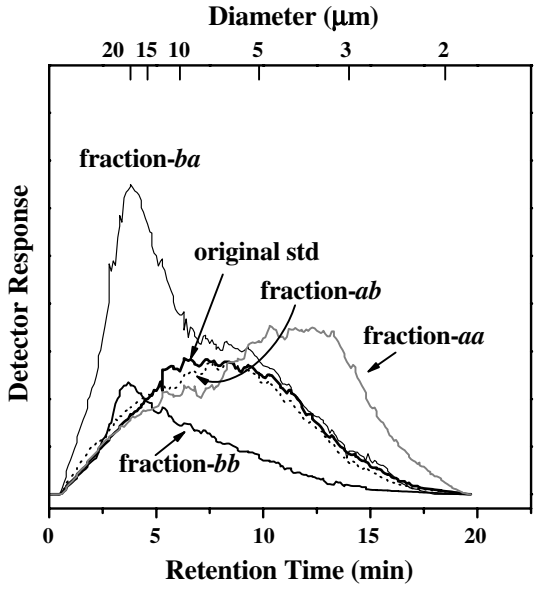


**Fig. 5** Sd/StFFF fractograms of the original IAEA-SED-1 and the four GSF fractions obtained from it at a rotation speed of 300 rpm. Flow rate was the same as that used in Fig. 4

The flow rate was the same as that used for the calibration.

As shown in Fig. 5, the elution profiles (and thus the size distributions) of the GSF fractions are quite different, and move to shorter elution time as the mean size decreases, as expected by the Sd/StFFF theory. It seems that retention of all the fractions is somewhat shorter than expected, thus yielding the apparent sizes larger than those measured by OM. This is probably because of the "shape effect" in Sd/StFFF, in which the non-spherical particles (flat or irregular shapes) are eluted earlier than spherical particles of the same mass, thus yielding a particle size distribution (converted from a fractogram using calibration data) for the non-spherical particles which seems to be shifted to the larger diameter scale [23].

It is noted that the signal from the UV–Vis detector in Sd/StFFF is mostly light scattered (a measure of turbidity rather than absorption) by the particles passing through the detector cell, and the signal intensity increases with increasing size and concentration. Thus the fractogram does not represent the size distribution accurately. Instead it represents the surface-area distribution of the eluted particles. To obtain an accurate PSD, light-scattering correction is required. The accurate scale factor compensating for the shape effect is not known and light-scattering correction was not performed in this work.

## Conclusion

Polydispersed and non-spherical sediment particles were analyzed by a combination of GSF and Sd/StFFF. Three-step GSF yielded four size-fractions of the particles on a semi-preparative scale. The particles were analyzed for size by Sd/StFFF. The size distributions of the GSF fractions were in reasonable agreement with theory despite the particles not being spherical. Results showed that a single GSF channel can be used for separation of particles of different cut-off diameters by using an appropriate combination of flow rates. It was also shown that accurate size analysis by Sd/StFFF for non-spherical particles requires full understanding of the "shape factor".

The combination of GSF and SdFFF is a useful combination for analysis of complex and polydispersed particulate samples, for example sea-sediment. GSF enables fractionation of the original sample into a few sub-groups based on size and/or density. The sub-groups can then be analyzed using either the normal or steric mode of SdFFF (Sd/NlFFF or Sd/StFFF) for more accurate characterization of the sample.

**Acknowledgements** This study was supported by the KOSEF (Korea Science & Engineering Foundation) Fund 1999-2-124-001-5.

## References

1. Giddings JC (1985) Sep Sci Technol 20:749–768
2. Jiang Y, Kummerow A, Hansen M (1997) J Microcol Sep 9:261–273
3. Contado C, Riello F, Blo G, Dondi F (1999) J Chromatogr A 845:303–316
4. Fuh CB (2000) Anal Chem 72:266A-271A
5. Moon MH, Kang DJ, Lee DW, Chang YS (2001) Anal Chem 73:693–697
6. Kim WS, Park M, Lee DW, Moon MH, Lim H, Lee S (2004) Anal Bioanal Chem 378:746–752
7. Moon MH, Kang DJ, Lim H, Oh JE, Chang YS (2002) Environ Sci Technol 36:4416–4423
8. Moon MH, Kang DJ, Lee DW, Chang YS (2001) Anal Chem 73:693–697
9. Giddings JS (1993) Science 260:1456–1465
10. Caldwell KD (1988) Anal Chem 60:959A-971A
11. Giddings JC, Ratanathanawongs SK, Barman BN, Moon MH, Liu G, Tjelta BL, Hansen ME(1993) Advances In: Bergna H (ed) chemistry series no. 234. ACS, Washington DC
12. Kim WS, Lee DW, Lee S (2002) Anal Chem 74:848–855
13. Lee JY, Lee S, Min YH, Hyun DY (2003) Bull Kor Chem Soc 24:1172–1176
14. Giddings JC (1988) Chem Eng News 66:34–45
15. Giddings JC, Ratanathanawongs SK, Moon MH (1991) KONA: Powder Part 9:200–217
16. Beckett R, Nicholson G, Hart BT, Hansen M, Giddings JC (1988) Water Res 22:1535–1545
17. Kim WS, Kim SH, Lee DW, Lee S, Lim CS, Ryu JH (2001) Environ Sci Technol 35:1005–1012
18. Moon MH, Lee S (1997) J Microcol Sep 9:565–570
19. Koch T, Giddings JC (1986) Anal Chem 58:994–997
20. Giddings JC, Moon MH, Williams PS, Myers MN (1991) Anal Chem 63:1366–1372
21. Moon MH, Giddings JC (1992) Anal Chem 64:3029–3037
22. Moon MH,Kim HJ, Kwon SY, Lee SJ, Chang YS, Lim H (2004) Anal Chem 76:3236 – 3243
23. Beckett R, Jiang Y, Moon MH, Liu G, Giddings JC (1994) Part Sci Technol 12:89–113